Mon. Not. R. Astron. Soc. **395,** 1249–1256 (2009) doi:10.1111/j.1365-2966.2009.14626.x

Constraining star formation and AGN in $z \sim 2$ massive galaxies using high-resolution MERLIN radio observations

C. M. Casey,[1⋆] S. C. Chapman,[1] T. W. B. Muxlow,[2] R. J. Beswick,[2] D. M. Alexander[3] and C. J. Conselice[4]

[1]*Institute of Astronomy, University of Cambridge, Madingley Road, Cambridge CB3 0HA*
[2]*Jodrell Bank Observatory, University of Manchester, Macclesfield SK11 9DL*
[3]*Department of Physics, University of Durham, South Road, Durham DH1 3LE*
[4]*School of Physics and Astronomy, University of Nottingham, University Park NG9 2RD*

Accepted 2009 February 9. Received 2009 February 9; in original form 2008 April 15

ABSTRACT

We present high spatial resolution Multi-Element Radio-Linked Interferometer Network (MERLIN) 1.4-GHz radio observations of two high-redshift ($z \sim 2$) sources, RG J123623 (HDF 147) and RG J123617 (HDF 130), selected as the brightest radio sources from a sample of submillimetre-faint radio galaxies. They have starburst classifications from their rest-frame ultraviolet spectra. However, their radio morphologies are remarkably compact (<80 and <65 mas, respectively), demanding that the radio luminosity be dominated by active galactic nuclei (AGN) rather than starbursts. Near-infrared (IR) imaging [*Hubble Space Telescope* Near Infrared Camera and Multi-Object Spectrometer (NICMOS) F160W] shows large-scale sizes ($R_{1/2} \sim 0.75$ arcsec, diameters ∼12 kpc) and spectral energy distribution (SED) fitting to photometric points (optical through the mid-IR) reveals massive ($\sim 5 \times 10^{11}\,\mathrm{M}_{\odot}$), old (a few Gyr) stellar populations. Both sources have low flux densities at observed 24 μm and are undetected in observed 70 μm and 850 μm, suggesting a low mass of interstellar dust. They are also formally undetected in the ultradeep 2 Ms *Chandra* data, suggesting that any AGN activity is likely intrinsically weak. We suggest both galaxies have evolved stellar populations, low star formation rates and low accretion rates on to massive black holes ($10^{8.6}\,\mathrm{M}_{\odot}$) whose radio luminosity is weakly beamed (by factors of a few). A cluster-like environment has been identified near HDF 130 by an overdensity of galaxies at $z = 1.99$, reinforcing the claim that clusters lead to more rapid evolution in galaxy populations. These observations suggest that high-resolution radio (MERLIN) can be a superb diagnostic tool of AGN in the diverse galaxy populations at $z \sim 2$.

Key words: galaxies: elliptical and lenticular, cD – galaxies: evolution – galaxies: individual: RG J123623 – galaxies: individual: RG J123617 – galaxies: starburst.

1 INTRODUCTION

The development of deep, multiwavelength imaging surveys has shed light on the rapid construction of galaxies and the build-up of stellar mass at high redshift ($z \sim 2$–3). The population of galaxies we see at this epoch is diverse – a testament to their rapid and significant growth. The cosmic star formation density peaks at this redshift ($z \sim 2$) as does the quasar space density (Fan et al. 2001; Blain et al. 2002; Richards et al. 2006). Galaxies at $z \sim 2$ display a wide range in properties, from negligible nuclear activity to the most powerful active galactic nuclei (AGN) and with star formation rates (SFRs) over $1000\,\mathrm{M}_{\odot}\,\mathrm{yr}^{-1}$ in Submillimetre Galaxies (SMGs; e.g. Blain et al. 2002) to as low as $1\,\mathrm{M}_{\odot}\,\mathrm{yr}^{-1}$ (e.g. quiescent galaxies; Cimatti et al. 2004; Daddi et al. 2004, 2005). Having also come to light in the past decade is the importance of AGN in regulating bulge growth (e.g. Di Matteo, Springel & Hernquist 2005). This is apparent in the local $M_{\star}$–M_{BH} relation where black hole mass is roughly ∼0.1 per cent of the spheroid's stellar mass (Kormendy & Richstone 1995; Magorrian et al. 1998; Gebhardt et al. 2000). This relationship clearly suggests that black hole mass and stellar mass build up symbiotically, with a broad range of $z \sim 2$ galaxies lying within a factor of a few of the local $M_{\star}$–M_{BH} ratio (e.g. McLure et al. 2006; Peng et al. 2006; Alexander et al. 2008b). Moderate-luminosity AGN with apparently low accretion efficiencies, ultraluminous AGN with powerful feedback winds, and heavily obscured, Compton thick AGN whose strength is shielded by dust in the host galaxy have been identified in galaxies with $L_{\mathrm{X}} > 10^{43}\,\mathrm{erg\,s}^{-1}$ at high z (Comastri 2004; Alexander et al. 2005,

⋆E-mail: ccasey@ast.cam.ac.uk

2008a; Brandt & Hasinger 2005; Daddi et al. 2007). Only through the most systematic searches of deep survey data may the full range of $z \sim 2$ galaxy properties be clearly understood.

In an effort to study an active subset of $z \sim 2$ galaxies, our collaboration has focused on the μJy radio galaxies, which are roughly 1/3 AGN, 1/3 submillimetre-bright star formers (SMGs) and 1/3 submillimetre-faint star formers (submillimetre-faint star forming radio galaxies, SFRGs). While most SMGs and SFRGs may have some contribution from low-luminosity AGN, their bolometric luminosity is dominated by dust-generated emission in the far-infrared (IR). The AGN sources have bolometric luminosities dominated by non-thermal radiation from AGN. SFRGs are likely to be the hotter dust counterparts of the SMG population (Chapman et al. 2004): the difference in their submillimetre properties is caused by a shift in the blackbody dust emission towards higher temperatures ($T_d > 50$ K). There is no other obvious physical difference between SFRGs and SMGs, both contributing significantly to the $z \sim 2$ star formation history (Casey et al. 2008). Here we present detailed multiwavelength studies of two galaxies, RG J123623 (HDF 147) and RG J123617 (HDF 130), originally identified as SFRGs but postulated here as being radio-bright but intrinsically low-luminosity AGN.

In Section 2 of this paper, we describe the observations and the parent sample from which the two galaxies are drawn. The observations include the Multi-Element Radio-Linked Interferometer Network (MERLIN) radio survey, Very Large Array (VLA) coverage of *Hubble Deep Field* (HDF), coverage by *Spitzer* 24 μm, 70 μm, *Hubble Space Telescope* photometry and morphology, and X-ray from *Chandra* Deep Field-North (CDF-N). In Section 3, we interpret these observations and derive an SED model, while in Section 4 we discuss the selection population and the possible physical scenarios that could describe such a set of multiwavelength observations, from a massive yet poorly accreting black hole whose radio emission is weakly beamed, to strongly beamed low-luminosity AGN and to heavily obscured Compton thick AGN. Throughout, we assume $H_0 = 70\,\mathrm{km\,s^{-1}}$, $\Omega_0 = 0.3$ and $\Omega_\Lambda = 0.7$.

2 SAMPLE AND OBSERVATIONS

HDF 147 and HDF 130 (see Table 1 for observation details) originate from a sample of 18 SFRGs (also referred to as 'OFRGs'; Chapman et al. 2004). The sample was defined by all radio-detected galaxies in seven distinct fields that were previously targeted in the submm by Submillimetre Common-User Bolometer Array (Holland et al. 1999) but lacked an optical counterpart brighter than $R = 23.5$. As described in Chapman et al. (2004), the requirement of an optically faint source eliminates low redshift, moderate-luminosity sources as well as high redshift, bright AGN and leaves a proposed population of predominantly hot dusty ultraluminous galaxies at $z \approx 2$. The set of SFRGs has much lower submillimetre flux densities (∼0.5 mJy) than the nominal ∼6.5 mJy of SMGs (e.g. Chapman et al. 2005).

High-resolution observations from the MERLIN (Thomasson 1986) were obtained for these sources as described in Muxlow et al. (2005). One motivation for the high angular resolution observations is distinguishing the compact emission of an AGN from more diffuse star formation, separating star-forming galaxies from AGN (e.g. Biggs & Ivison 2008). Muxlow et al. (2005) discuss the 0.3–0.5 arcsec beamsize MERLIN observations in depth. The rms noise from MERLIN data was 5.9 μJy beam^{-1}. The images from the VLA (Richards et al. 1999; Richards 2000) and MERLIN were combined in the image plane and used to make a sensitive 1.4-GHz map with high positional accuracy (tens of mas) allowing high-resolution imaging and identification of μJy sources (Biggs & Ivison 2006, 2008).

Table 1. Physical properties of HDF 147 and HDF 130.

	HDF 147	HDF 130
RA (J2000)	12:36:23.54	12:36:17.55
DEC (J2000)	+62:16:42.8	+62:15:40.8
redshift	1.918	1.993
VLA $S_{1.4\,\mathrm{GHz}}$	481.0 ± 25.4 μJy	200.0 ± 12.8 μJy
WSRT $S_{1.4\,\mathrm{GHz}}$	476 ± 31 μJy	375 ± 28 μJy
$S_{850\,\mu\mathrm{m}}$	1.6 ± 1.1 mJy	2.1 ± 1.0 mJy
$S_{70\,\mu\mathrm{m}}$	<2.1 mJy	<1.9 mJy
$S_{24\,\mu\mathrm{m}}$	18 ± 3 μJy	24 ± 3 μJy
8.0 μm mag	20.45 ± 0.59	21.48 ± 0.95
5.8 μm mag	19.76 ± 0.74	20.77 ± 1.17
4.5 μm mag	19.57 ± 0.32	20.58 ± 0.52
3.6 μm mag	19.63 ± 0.31	20.72 ± 0.52
B mag	>25.7	25.4 ± 1.0
V mag	>26.5	25.3 ± 1.0
I mag	25.9 ± 1.0	25.1 ± 1.0
Z mag	24.6 ± 0.5	24.7 ± 0.5
H mag	21.2 ± 0.5	22.5 ± 0.6
$L_{\mathrm{X,(0.5-8.0\,keV)}}$	4.1×10^{42} erg s^{-2}	$<8.2 \times 10^{42}$ erg s^{-2}
$R_{1/2}$ (H band)	8.65 kpc (1.02 arcsec)	3.7 kpc (0.44 arcsec)
$R_{1/2}$ (MERLIN)	<680 pc (<80 mas)	<550 pc (<65 mas)
$\log(M_\star/\mathrm{M}_\odot)$	$11.8^{+0.3}_{-0.3}$	$11.4^{+0.4}_{-0.2}$
$\log(M_{\mathrm{BH}}/\mathrm{M}_\odot)$	$8.9^{+0.6}_{-0.6}$	$8.5^{+0.7}_{-0.5}$
$\rho_\star(M_\odot\,\mathrm{kpc}^{-3})$	$1.2^{+1.1}_{-0.6} \times 10^8$	$5.7^{+8.7}_{-2.1} \times 10^8$
n (Sersic Index)	3.5 ± 0.3	1.5 ± 0.5
H-band axis ratio	0.66	0.98
$E(B-V)$	0.40	0.03
Lyα/C IV	0.75 ± 0.06	1.67 ± 0.03
Lyα/He II	0.62 ± 0.06	1.67 ± 0.02

Notes – All magnitudes are in the AB-magnitude system. X-ray luminosity is given for the rest-frame 0.5–8.0 keV band. The variable $R_{1/2}$ denotes the half light radius of the galaxy in H band and MERLIN radio imaging, respectively. The Sersic Exponent, n, refers to the GALFIT profile fitting to H band. The derived quantities come from calculations described in Section 3.

Spitzer observations were made in Infra Red Array Camera (IRAC) 3.6, 4.5, 5.8 and 8.0 μm and Multiband Imaging Photometer for Spitzer (MIPS) 70 μm (Frayer et al. 2006) and 24 μm bands in the HDF region (PI M. Dickinson; Chary et al., in preparation). This component of observations is used to study the galaxies' stellar masses. Optical imaging of the area is from the HDF,[1] in B (F435W), V (F606W), i (F814W) and z (F850LP) bands all in the AB magnitude system. As part of the extensive 45 arcmin^2 near-IR survey coinciding with the HDF and Great Observatories Origins Deep Survey-North (GOODS-N), we have obtained NICMOS imaging using NIC3 three-orbit pointing in F160W of both HDF 147 and HDF 130 (Conselice et al., in preparation).

The parent sample of SFRGs was also observed spectroscopically with Keck/Low Resolution Imaging Spectrometer (LRIS) (Oke et al. 1995; Steidel et al. 2004) from 2002 to 2004. Full details of these rest-ultraviolet (UV) spectral observations are found in Chapman et al. (2004). In short, the galaxies'

[1] Based on observations made with the NASA/ESA *Hubble Space Telescope* and obtained from the Hubble Legacy Archive, which is a collaboration between the Space Telescope Science Institute (STScI/NASA), the Space Telescope European Coordinating Facility (STECF/ESA) and the Canadian Astronomy Data Centre (CADC/NRC/CSA).

redshifts were identified by detection of several emission features (Lyα and C IV in the case of HDF 147 and Lyα and He II in the case of HDF 130). Although their spectra are faint (see fig. 2 of Chapman et al.), both resemble starburst galaxies, so we grouped them originally in the parent SFRG sample. We attempted to measure individual line fluxes from several features that would more clearly classify HDF 147/HDF 130 as starbursts or AGN, but the spectra are too faint to go beyond the analysis of Chapman et al. (2004).

Observations in the X-ray are from the 2 Ms CDF-N (Alexander et al. 2003), centred on the HDF in the 0.5–8.0 keV band which achieves an aim-point sensitivity of $\approx 1.2 \times 10^{-16}$ erg cm^{-2} s^{-1}. X-ray observational details of a similar SMG population are found in Alexander et al. (2005). At the redshifts of these galaxies ($\sim$1.96), the observed 0.5–8.0 keV band corresponds to rest-frame energies 1.5–24 keV. Neither galaxy is listed in the Alexander et al. (2003) catalogue; however, HDF 147 is marginally detected at a low significance in the narrow 1–2 keV band (a luminosity of 1.67×10^{42} erg s^{-1} in the observed 0.5–8 keV band). Assuming an average X-ray spectral slope $\Gamma = 1.8$, we find the luminosity of HDF 147 in the rest 0.5–8.0 keV band is $L_{\rm X(HDF\,147)} = 4.1 \times 10^{42}$ erg s^{-1} and the 3-σ upper limit for HDF 130 is $L_{\rm X(HDF\,130)}(2\text{–}10\,{\rm keV}) \leq 8.2 \times 10^{42}$ erg s^{-1}.

3 ANALYSIS AND RESULTS

3.1 Constraining star formation

The measurement of the radio angular sizes of HDF 147 and HDF 130 was made using the AIPS software, JMFIT. JMFIT was used to fit a single 2-d Gaussian to the core component of each galaxy in the CLEANed MERLIN plus VLA radio image restored with a 200 mas circular beam. Subsequently, the restoring beam of this image was deconvolved from these fitted sizes. The radio images of both HDF 130 and HDF 147 are of high signal-to-noise ratio and close to the pointing centre, thus the measurement of deconvolved radio sizes several times smaller than the restored CLEAN beam of the image can be reliably made (e.g. Condon et al. 1998). The fitted sizes, deconvolved with the image restoring beam, of the cores of HDF 147 and HDF 130 are <80 and <65 mas, respectively, with an error on the fitted full width at half-maximum of 20 mas (Condon 1997). At these redshifts, these angular size limits correspond to linear sizes of <640 and <520 pc.

Fig. 1 shows contoured images of HDF 147 and HDF 130 overlaid on Advanced Camera for Surveys (ACS)/NICMOS imaging. Muxlow et al. (2005) classify HDF 147 (J123623+621642) as an AGN candidate and note that it has a faint one-sided radio emission extending ∼0.6 arcsec to the south of the compact core. This core and jet-like emission can clearly be seen in Fig. 1. The radio structure of HDF 130 (J123617+621540) is compact in the high-resolution images presented here, however from lower resolution (0.5 arcsec) imaging of these data Muxlow et al. (2005) showed this source to have compact core with two-sided radio emission extending over a linear extent of 1.3 arcsec. The HDF 147 radio morphology of Fig. 1 exhibits a low luminosity (∼20 μJy) extension along the galaxy's minor axis. This is a possible candidate for radio jet outflows but provides no obvious clue to source orientation.

If star formation were the source of radio emission, both sources would exceed the maximum star formation density possible for a given mass and dynamical time-scale (Elmegreen 1999). HDF 147 and HDF 130 have limits on their radio size smaller than most local ultra-luminous infrared galaxy (ULIRGs). As local ULIRGs with

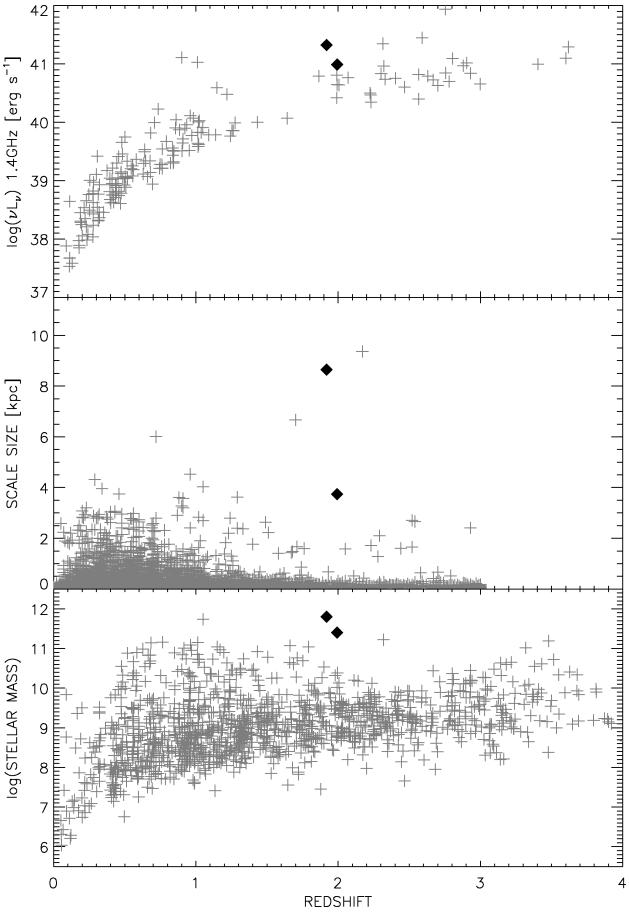

Figure 1. Radio luminosity (Chapman et al. 2003), scale sizes (Abraham, van den Bergh & Nair 2003; Abraham et al. 2004) and stellar mass (Conselice, Blackburne & Papovich 2005; Conselice, Rajgor & Myers 2008) against redshift for radio galaxies in several large survey fields. HDF 130 and HDF 147 are highlighted as black diamonds at much larger radio luminosities, scale sizes and higher masses than are typical high-z galaxies.

$\Sigma_{\rm SFR} \sim 200\,{\rm M}_\odot\,{\rm yr}^{-1}\,{\rm kpc}^{-2}$ are already forming stars near a theoretical maximum (e.g. Tacconi et al. 2006), HDF 147 and HDF 130 would exceed this limit by factors of 50–70× given that their radio-inferred SFR densities are 15 000 and 11 000 $\rm M_\odot\,yr^{-1}\,kpc^{-2}$, respectively (with only small variations due to geometry and gas fractions). We therefore conclude that the radio emission we observe must be largely emitted by AGN.

We further constrain their SFRs using the rest-UV luminosities (equation 1 of Kennicutt 1998). Without removing the effects of dust extinction, we constrain HDF 147 to a maximum[2] SFR of $5^{+4}_{-2}\,{\rm M}_\odot\,{\rm yr}^{-1}$ and HDF 130 to an SFR of $17^{+6}_{-4}\,{\rm M}_\odot\,{\rm yr}^{-1}$. Corrected for extinctions of $E(B-V) = 0.40$ and 0.03, respectively[3] (calculated from HYPERZ stellar population model fits, as described in the next section), the UV SFR constraints are $\rm SFR_{HDF\,147} = 110^{+88}_{-44}\,M_\odot\,yr^{-1}$ and $\rm SFR_{HDF\,130} = 22^{+8}_{-6}\,M_\odot\,yr^{-1}$. The low 24 and 850 μm luminosities are consistent with these SFRs ($S_{850} \leq 2$ mJy; SFR $< 300\,{\rm M}_\odot\,{\rm yr}^{-1}$).

[2] If all of the UV emission were from star formation.

[3] We considered the effect of inter-galactic medium (IGM) extinction at $z \sim 2$, but found it was insignificant compared to magnitude uncertainty and extinction internal to the galaxies.

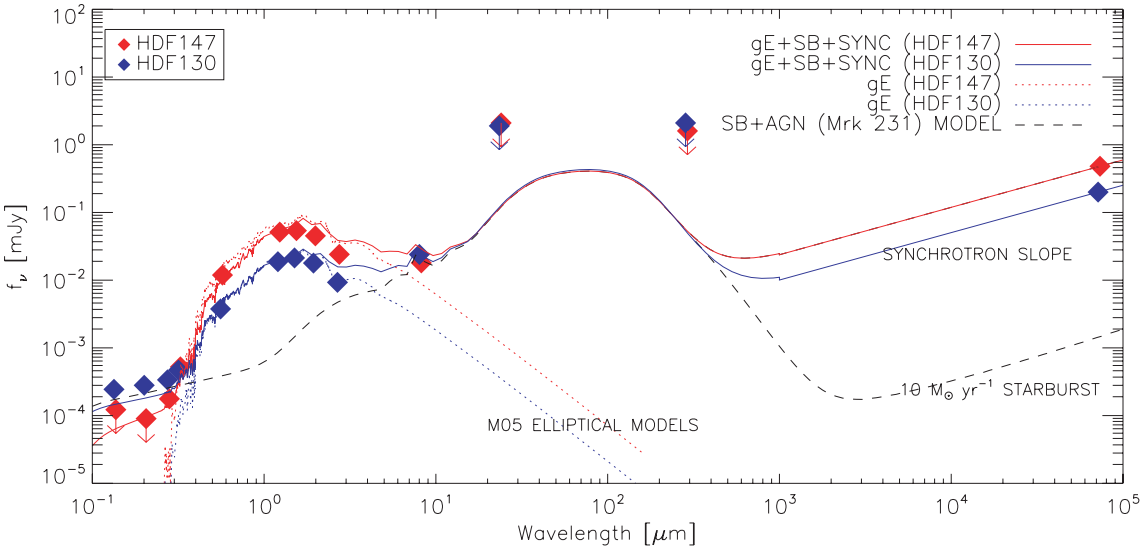

Figure 2. A composite SED for the two galaxies (red for HDF 147, blue for HDF 130) in rest wavelength, from UV through the IR, submillimetre and radio. The old stellar populations, adapted from Maraston (2005) stellar evolution models, are fit to the optical and *Spitzer-IRAC* photometry, around the rest-1.6 μm stellar bump (dotted lines labelled 'M05 Elliptical Models'). A Calzetti dust extinction law (e.g. Calzetti, Kinney & Storchi-Bergmann 1994) is used to extinct the flux in the UV, with derived reddening factors of $E(B-V) = 0.40$ and $E(B-V) = 0.03$ for HDF 147 and HDF 130, respectively. A Mrk 231 template SED (Berta 2006), scaled to the 24-μm flux densities, is added to represent the far-IR and radio portion of the SED. We fit the SED to the radio points by scaling up the emission from synchrotron emission ($\alpha = 0.7$) from the nominal flux densities that were expected from the Mrk 231 template (dashed line).

3.2 Characterizing the stellar populations

To learn about the stellar components of HDF 147 and HDF 130, we fit the optical and *Spitzer-IRAC* photometric points to stellar population templates from Maraston (2005) using the HYPERZ package (Bolzonella, Miralles & Pelló 2000). HYPERZ output includes internal extinction factor A_V and rest K-band absolute magnitude, which we use to calculate extinction-corrected UV SFRs and derive stellar masses, respectively. The Maraston model populations assume a Salpeter initial mass function and range in age from 10 Myr to 15 Gyr.[4] We find that the older models (10–15 Gyr) are much better fits to both galaxies' photometry than a 'young' model aged only a few Gyrs. Furthermore, we find that the instantaneous starburst models with 0.67 metallicity fit best, where goodness of fit is measured by minimizing the χ^2 statistic.

We measure extinction factors $A_V = 1.3$ for HDF 147 and $A_V = 0.1$ for HDF 130, which corresponds to $E(B-V)_{147} = 0.40$ and $E(B-V)_{130} = 0.03$. These derived values are used to estimate the rest-UV SFRs described in the previous section.

We have used the methodology outlined in Borys et al. (2005) to estimate stellar masses from rest-frame K-band magnitudes, which we measured from HYPERZ to be −26.67 for HDF 147 and −26.81 for HDF 130. We assume a mass-to-light ratio of $L_K/M = 1.9$ because of the galaxies' predominantly old stellar populations ($\tau > 1$ Gyr). Both galaxies are exceptionally massive, with $\log(M/\mathrm{M}_\odot) = 11.8^{+0.3}_{-0.3}$ and $11.4^{+0.4}_{-0.2}$ for HDF 147 and HDF 130, respectively. The contrast to other $z \sim 2$ galaxies is seen in panel 3 of Fig. 1. We use the well-studied local $M_\star$–$M_{\rm BH}$ relation where $M_{\rm BH} = M_\star/1000$ (Kormendy & Richstone 1995; Magorrian et al. 1998; Gebhardt et al. 2000) to estimate black hole masses of $\log(M_{\rm BH}/M_\odot) = 8.9^{+0.6}_{-0.6}$ and $8.5^{+0.7}_{-0.5}$, with the caveat that there is a factor of 2 variation in the $M_{\rm BH}/M_\star$ ratio. We caution that $M_\star$–$M_{\rm BH}$ has a larger spread and is slightly elevated at $z \sim 2$ than locally (e.g. McLure et al. 2006; Peng et al. 2006) although such variation could be caused by a bias towards large black holes (Lauer et al. 2007; Alexander et al. 2008b).

Fig. 2 explores SED fitting for these galaxies from the rest-UV wavelengths to the radio. The SED shortward of 1 μm is dominated by the best-fitting HYPERZ Maraston stellar population models (dotted lines in Fig. 2). Towards longer wavelengths, we introduce a template Mrk 231 SED (adapted from Berta 2006) including both AGN and moderate star former components and normalize it to the 24-μm flux densities (dashed line in Fig. 2). The inferred SFR from templates with this 24 μm normalization is $\sim$10 $\mathrm{M}_\odot$ yr^{-1}. We then raise the radio synchrotron contribution to the SED (but we keep the synchrotron slope, $\alpha = 0.7$ the same) to fit the galaxies' bright radio luminosities.

The optical to mid-IR portion of the SED provides a good fit to the data: a sum of old and massive stellar populations with moderate ($\sim$10 $\mathrm{M}_\odot$ yr^{-1}) star formation. The submillimetre flux density limits do not place any significant additional constraints on the SEDs. In the rest-UV (B and V bands) HDF 147 is undetected. HDF 130 exhibits a moderate blue excess, with associated SFR = 22 $\mathrm{M}_\odot$ yr^{-1}, which may correspond to the starburst detected in its rest-UV spectrum. We emphasize that the total luminosity from the star-forming component is minor compared to the very luminous SED-characterized '1.6 μm-bump' stellar population.

3.3 Size and morphological classification

In contrast to optical imaging, NICMOS near-IR imaging reveals that the galaxies have half light radii of 8 and 4 kpc, over 20 times the scale of the radio core emission. This is shown in Fig. 3. van Dokkum et al. (2008) find that while local galaxies have a typical size of $R_{1/2} \sim 5$ kpc, elliptical galaxies of $\sim 3 \times 10^{11}$ $\mathrm{M}_\odot$ at $z \sim 2.3$ are much more compact with average $R_{1/2} = 0.9$ kpc, which is significantly smaller than HDF 147 and HDF 130 (see Fig. 1, panel 2). However, the stellar densities of HDF 147 and HDF 130

[4] Although the age of the Universe is only $\sim$13.7 Gyrs, the aging of the Maraston stellar population models has not been normalized to the current cosmology, thus allowing '15 Gyr' old models.

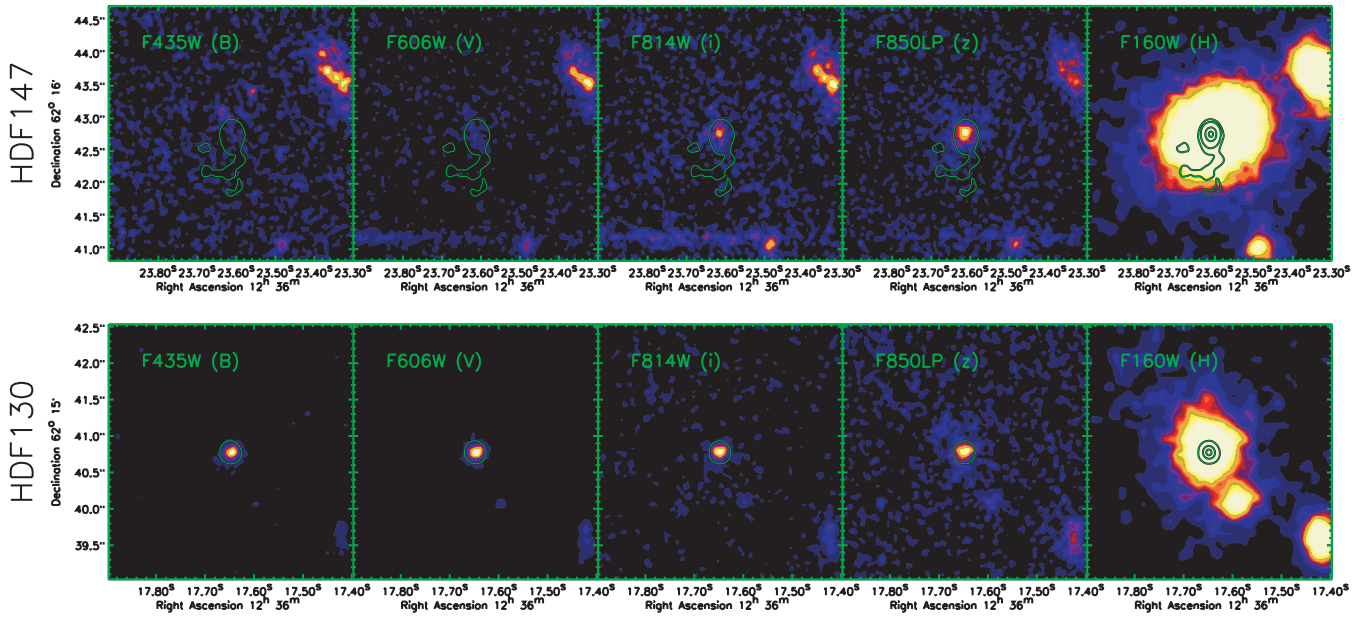

Figure 3. MERLIN radio contours overlayed with ACS *B, V, i, z* (F435W, F606W, F814W, F850LP) and NICMOS H (F160W) imaging of galaxies HDF 147 (top) and HDF 130 (bottom). HDF 147 shows a faint extended region to the north of the radio and NICMOS centres; its NICMOS size is substantially larger than most galaxies at its epoch at a ∼17 kpc diameter. HDF 130 has compact blue emission which is coincident with the radio centre, but has a much more extended morphology, ∼8 kpc across, in *H* band. The ACS panels show only the 15 μJy radio contour for clarity while the NICMOS panels show more complete contours: 15, 40, 150, 255 and 380 μJy. The peak flux density of HDF 147 is 423 μJy and for HDF 130 it is 162 μJy.

($\rho_{\star,147} = 1.2^{+1.1}_{-0.6}\,\mathrm{M}_\odot\,\mathrm{kpc}^{-3}$, $\rho_{\star,130} = 5.7^{+8.7}_{-2.1}\,\mathrm{M}_\odot\,\mathrm{kpc}^{-3}$[5]) are much lower than the high-density $z \sim 2.3$ galaxies and similar to local ellipticals (Blanton et al. 2005). A similar size comparison of massive ($M > 10^{11}\,\mathrm{M}_\odot$) high z ($1.7 < z < 2.0$) galaxies from Trujillo et al. (2007) also shows that HDF 147 and HDF 130 are much larger than typical quiescent galaxies at similar redshifts. Trujillo et al. (2007) find that for galaxies with large Sersic index ($n > 2.5$) the expected size is $R_{1/2} = 1.1 \pm 0.4$ kpc and for shallower potentials ($n < 2.5$) it is $R_{1/2} = 2.3 \pm 1.8$ kpc.

We fit Sersic profiles to *H*-band imaging to search for substructure, derive Sersic indices and model their morphologies. Fitting both HDF 147 and HDF 130 using GALFIT (Peng et al. 2002), we find that HDF 147 closely resembles a de Vaucouleurs profile ($n = 3.5 \pm 0.3$) while HDF 130 fits well to a more extended exponential ($n = 1.5 \pm 0.5$). Clearly by this analysis, HDF 147 is a giant elliptical galaxy with smooth morphology and $R_e \sim 9$ kpc. HDF 130 is near the boundary between elliptical galaxies and disc-like structures at $n = 1.5$ and shows no substructure; its giant size, giant mass, lack of significant star formation ($<100\,\mathrm{M}_\odot\,\mathrm{yr}^{-1}$) and old stellar population are characteristic of large quiescent galaxies.

3.4 Environment characterization and further classification

Given the large stellar masses, old stellar populations and large-scale sizes of these galaxies, the question of their environment naturally arises since locally giant elliptical (gE) galaxies reside exclusively in highly clustered environments. Blain et al. (2004) observed that there was a strong association of five SMGs in this field at the redshift $z \sim 1.99$ (around HDF 130), representing the largest *cluster* of SMGs in the Chapman et al. (2005) spectroscopic survey. Chapman et al. (2009) have studied this structure further showing that an overdensity of galaxies of all types exists at this redshift, although not with the same degree of contrast as the SMGs. No such structure was found associated with HDF 147, although it is possible that one exists and has not been observed due to spectroscopic incompleteness.

The Bauer et al. (2002) study of extended X-ray sources detects elongated X-ray emission roughly centred on HDF 130 (CDF-N source 2, scale size ∼1 arcmin; see their fig. 2 most upper-right panel). Due to its double-lobed shape and sharp cut-off on the ends, the emission could be due to inverse Compton scattering of the cosmic microwave background due to AGN outflow in HDF 130 rather than the cooling gas of an extended cluster. The size of the emission region is 300–500 kpc and no radio lobes or plumes are observed to correlate with the X-ray region. Detailed analysis of the X-ray observations of this region is presented in Fabian et al. (2009).

These galaxies were not selected as $z = 2$ BX/BM objects by Steidel et al. (2004) from their colours and they do not appear in the spectroscopic catalogues of Cowie et al. (2004). Both galaxies satisfy the *p-BzK* selection criteria for passively evolving galaxies ($BzK < -0.2$, $z - K > 2.5$) as described by Daddi et al. (2004). However, the scale size of these galaxies is much larger than the vast majority of p-BzK galaxies which are generally very compact (scale radii <0.9 kpc; van Dokkum et al. 2008).

4 DISCUSSION

To understand the importance of galaxies like HDF 147 and HDF 130 at $z \sim 2$, we first characterize the parent sample of radio sources from which they were selected. We illustrate schematically in Fig. 4 the relative fractions of different galaxies (SMGs, SFRGs and AGN) comprising the μJy $z \sim 2$ radio galaxy population (a more detailed analysis is in Casey et al. 2008). HDF 147

[5] The mean stellar density within the half light radius, $\rho_\star = 0.5M/[(4/3)\pi R^3_{1/2}]$.

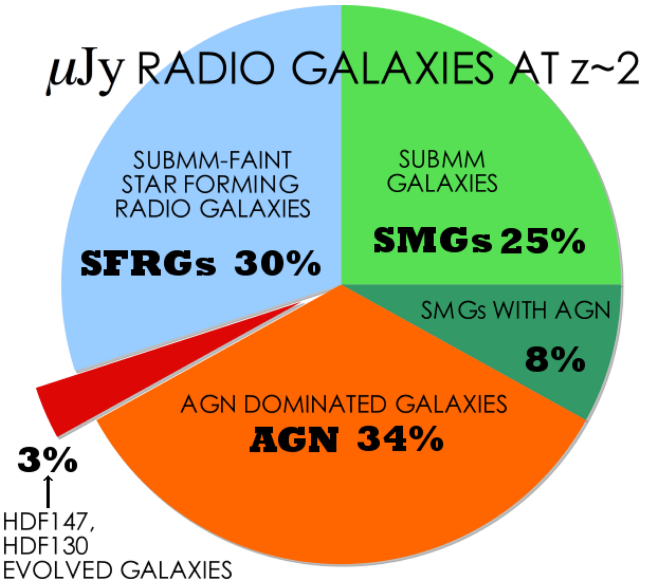

Figure 4. A schematic pie chart characterizing the $z \sim 2$ μJy radio source population. SMGs and SFRGs have optical spectra consistent with starbursts, while AGN and SMGs with AGN have spectral signatures of AGN. The SMGs and SMGs with AGN are detected at 850 μm. HDF 147 and HDF 130 are highlighted as the small red slice, between SFRGs and AGN; while they were previously diagnosed as SFRGs from their spectra, we have shown that they are more appropriately classified as AGN.

and HDF 130 are highlighted since our observations have demonstrated that they should be classified as AGN-dominated rather than star formation-dominated SFRGs. These two galaxies represent a rare type of massive galaxy with an estimated volume density of $1.5 \times 10^{-6}\,\mathrm{Mpc}^{-3}$ (given two objects detected in a well-studied area $15 \times 15\,\mathrm{arcmin}^2$ and redshift range $1.8 < z < 2.6$). Evolved elliptical galaxies of this type (with stellar masses over $10^{11}\,\mathrm{M}_\odot$ and negligible black hole accretion) are extremely rare at high redshift. Conselice et al. (2007) estimate $\Phi \ll 5 \times 10^{-6}\,h_{70}^3\,\mathrm{Mpc}^{-3}$ the volume density estimate for highly evolved $z \sim 2$ galaxies, which is less than Φ for SMGs (Chapman et al. 2003). While this suggests a quite sparse population, a combination of spectroscopic incompleteness in the radio source population and a possible wider range of physical properties consistent with these two galaxies could suggest that they are an important evolutionary stage of massive galaxies.

This section explores physical explanations for the observational constraints: high-resolution radio indicating the presence of an AGN, low X-ray luminosities, no evidence for high-ionization UV emission lines and low 24 μm luminosities.

4.1 Evolved galaxies with poorly accreting black holes?

The observational constraints (low 24 μm and X-ray luminosities) require that there be very little accretion ($\eta \ll 0.1$) on to the massive $10^{8.9}$ and $10^{8.5}\,\mathrm{M}_\odot$ black holes. This lower accretion efficiency could be explained by decreased fuelling of the AGN, where most cool gas has been converted into stars or expelled from the elliptical galaxies by feedback mechanisms. A lack of hot AGN torus dust is a condition for this interpretation because of the weak mid-IR luminosity.

With low X-ray luminosities yet high radio luminosities, we suggest these radio fluxes may be boosted by some mechanism. We propose weak radio beaming, here defined as jet-line of sight orientation angles less than 30° with fluxes boosted by a factor of a few, to explain the 200–500 μJy radio flux densities. At the other extreme, referring back to Fig. 2, we see that the radio emission inferred from a moderate-luminosity AGN with modest star formation would be ∼2 μJy. The intrinsic emission of the HDF 147/HDF 130 AGN components must lie between 2 and 200 μJy.

We suggest that HDF 147 and HDF 130 are likely the high-redshift analogue of local Fanaroff–Riley I's (FR I; Fanaroff & Riley 1974), which we use to estimate volume density and the probability of our observations. Both galaxies fall below the critical FR I/FR II boundary in radio luminosity and rest-frame optical magnitude (i.e. the radio-optical magnitude bivariate FR I/FR II boundary; Ledlow & Owen 1996). They are also classified as FR I's in the original classification scheme [i.e. $L < L_{\mathrm{CRIT}}(178\,\mathrm{MHz}) \approx 2 \times 10^{25}\,\mathrm{W\,Hz^{-1}\,str^{-1}}$ assuming $\alpha = 0.8$; Fanaroff & Riley 1974]. Their intrinsic emission is likely similar to the average luminosity of these nearby FR I AGN in evolved galaxies with $\nu L_\nu(1.4\,\mathrm{GHz}) \sim 5 \times 10^{39}\,\mathrm{erg\,s^{-1}}$. The probability of observing intrinsic radio luminosities of $\nu\ L_\nu\ (1.4\,\mathrm{GHz}) \sim 10^{41.3}\,\mathrm{erg\,s^{-1}}$ among FR I radio sources is very low (Ledlow & Owen 1996): 0.5 per cent (to observe HDF 147 at $\nu\ L_\nu = 10^{41.5}$) and 1.3 per cent (to observe HDF 130 at $\nu\ L_\nu = 10^{41.1}$). Both probabilities represent the fraction of FR Is in the Ledlow & Owen sample with that luminosity or greater. If we allow beaming in both cases so that intrinsic luminosities drop by a factor of 10, then the probability of our observation increases marginally by 5 times. We caution that the statistics behind the Ledlow & Owen (1996) sample are limited and only include nearby sources and that the evolution with redshift might not be constant.

We can also use the much larger and well-studied statistics of the faint-end quasar luminosity function (QLF) and apply constraints based on different beaming-strength geometries. The most recent studies of the QLF are from Richards et al. (2006) and Hopkins, Richards & Hernquist (2007), whose faint-end reliabilities, as they relate to probable low-luminosity low-accretion rate AGN, are discussed in Casey et al. (2008). For $26.5 < i < 23.5$ (the magnitude selection cut on the parent sample of SFRGs) and $1.7 < z < 2.3$, the AGN surface density is $168 \pm 2\,\mathrm{deg}^{-2}$. Assuming an isotropic distribution in orientation angles for type 1 AGN, the number of these faint AGN whose jets are pointed towards Earth within 30° (weak-beaming) is $42 \pm 17\,\mathrm{deg}^{-2}$. For strong beaming (<3° opening angle, ∼100 amplification), the numbers shrink to $0.8 \pm 0.3\,\mathrm{deg}^{-2}$. We therefore expect 1.2 ± 0.5 low-luminosity, weakly beamed AGN to appear in the MERLIN coverage of GOODS-N, which agrees with the two galaxies we have found.

Since we classify these galaxies as massive, with old stellar populations, there is also a constraint on X-ray emission produced by hot gas that we test. While all massive ellipticals in the local Universe have large quantities of X-ray emitting gas (as have been shown out to $z = 0.7$ in Lehmer et al. 2007), the expected X-ray luminosity from hot gas in these systems is about an order of magnitude below the current *Chandra* X-ray limits ($L_{\mathrm{X}} \sim 10^{41}\,\mathrm{erg\,s^{-1}}$).[6]

4.2 Alternate hypotheses

The possibility exists that HDF 147/HDF 130 are highly beamed (opening angle < 3°) low-luminosity AGN. This hypothesis would further reduce the concern for low dust masses in a hot torus since

[6] The hot-gas X-ray constraints were calculated using the average X-ray to *K*-band luminosity ratio of early type galaxies from Ellis & O'Sullivan (2006) and Lehmer et al. (2007, 2008).

low-luminosity AGN would not create significant re-radiated mid-IR flux even in the presence of dense dust clouds. However, looking straight down the radio jets, one would expect signs of a BL Lac type optical spectrum, which is clearly not present. A variation on the low-luminosity AGN hypothesis is that the central black holes are much less massive than the local $M_\star$–$M_{\rm BH}$ predicts. The lower mass limits determined by Eddington-limited accretion are $10^{5.9}$ and $<10^{6.1}\,{\rm M}_\odot$ (two orders of magnitude below the predictions of $M_\star$–$M_{\rm BH}$, as in fig. 3 of Borys et al. 2005). However, under this hypothesis we would have to advocate factors $>100\times$ beaming to boost the radio luminosity above what is expected for such small black holes (e.g. Merloni, Heinz & di Matteo 2003). With the analysis of the previous subsection, the orientation geometry is likely implausible for either variation of the highly beamed, low-luminosity AGN hypothesis (with probability $\ll$1 per cent, requiring both galaxies to have jet-line of sight orientation angles of $<3^\circ$).

Compton thick AGN are also an alternate hypothesis. The lack of detection in the soft X-ray could be explained by a deeply buried, obscured AGN. The extreme obscuration could also explain the weak rest-UV. The AGN would permeate the dust obscuration in the radio, however one would expect a much higher 24 μm flux density due to a high dust content (by at least an order of magnitude Alexander et al. 2008b).

5 CONCLUSIONS

We have presented multiwavelength observations of two high-redshift galaxies, arguing that they are highly evolved giant elliptical galaxies with low-luminosity, beamed AGN. Their near-IR morphologies (NICMOS H band) show giant elliptical characteristics typical of an old stellar population whose stellar bump is well characterized in the IRAC filters. The physical sizes of both galaxies are 2–5 times larger than most evolved galaxies at the same redshift, and similarly the stellar masses are large, around $\sim 4 \times 10^{11}\,{\rm M}_\odot$. By the $M_\star$–$M_{\rm BH}$ relation, we infer black hole masses $\sim 3 \times 10^8\,{\rm M}_\odot$. The lack of strong AGN suggests accretion at very low rates. Without X-ray detections and without strong power-law continua in the rest-UV, we assume they are low-luminosity AGN whose radio emission must be beamed by a factor of a few. We offer discussions of other possible scenarios, but it is most likely that we are observing evolved galaxies with AGN that have nearly exhausted their fuel source. While this type of highly evolved galaxy is rare at high z, the supplemental knowledge that galaxy overdensities have been found near $z = 1.99$ in the HDF reinforces, if only slightly, the notion that galaxy evolution occurs more rapidly in cluster environments.

These galaxies were originally classified as radio-selected star formers, likely with hotter dust temperatures than their SMG counterparts because of their 850-μm non-detections. Only their compact MERLIN radio morphologies and weak 24-μm flux set them apart from high-SFR galaxies. A full analysis of the SFRG population is in Casey et al. (2008). The planned eMERLIN deep pointings at 1.4 and 5 GHz in GOODS-N will push detections to $\sim$0.5 μJy rms, measuring radio spectral indices and spatially separating emission from AGN and star formation.

So far, these galaxies have gone unnoticed in an otherwise well-studied deep survey field. The potential to study more galaxies exhibiting the same properties is possible, as many have probably gone un-noted in studies due to incredibly faint X-ray and optical fluxes. Although both objects were measured at 1.4 GHz with the VLA, it was the MERLIN high-resolution coverage which distinguished the extreme radio luminosities as emanating from the extremely compact galaxy cores. If HDF 147 and HDF 130 contain beamed low-luminosity AGN as we propose, they provide a test bed for understanding evolved and poorly accreting systems at high redshift.

ACKNOWLEDGMENTS

We thank the anonymous referee for insightful comments and suggestions which helped improve the paper. We thank Chris Simpson for his advice on the AGN components of HDF 147 and HDF 130, Andy Fabian for his input on the extended inverse Compton emission associated with HDF 130 and Bret Lehmer for his input on the X-ray emission from hot gas in both galaxies. CMC thanks the Gates–Cambridge Trust for support and DMA thanks the Royal Society.

REFERENCES

Abraham R. G., van den Bergh S., Nair P., 2003, ApJ, 588, 218
Abraham R. G. et al., 2004, AJ, 127, 2455
Alexander D. M. et al., 2003, AJ, 126, 539
Alexander D. M., Bauer F. E., Chapman S. C., Smail I., Blain A. W., Brandt W. N., Ivison R. J., 2005, ApJ, 632, 736
Alexander D. M. et al., 2008a, ApJ, 687, 835
Alexander D. M. et al., 2008b, AJ, 135, 1968
Bauer F. E., Alexander D. M., Brandt W. N., Hornschemeier A. E., Vignali C., Garmire G. P., Schneider D. P., 2002, AJ, 124, 2351
Berta S., 2006, PASP, 118, 754
Biggs A. D., Ivison R. J., 2006, MNRAS, 371, 963
Biggs A. D., Ivison R. J., 2008, MNRAS, 385, 893
Blain A. W., Smail I., Ivison R. J., Kneib J.-P., Frayer D. T., 2002, Phys. Rep., 369, 111
Blain A. W., Chapman S. C., Smail I., Ivison R., 2004, ApJ, 611, 725
Blanton M. R. et al., 2005, AJ, 129, 2562
Bolzonella M., Miralles J.-M., Pelló R., 2000, A&A, 363, 476
Borys C., Smail I., Chapman S. C., Blain A. W., Alexander D. M., Ivison R. J., 2005, ApJ, 635, 853
Brandt W. N., Hasinger G., 2005, ARA&A, 43, 827
Calzetti D., Kinney A. L., Storchi-Bergmann T., 1994, ApJ, 429, 582
Casey C. M. et al., 2008, ApJS, 177, 131
Chapman S. C. et al., 2003, ApJ, 585, 57
Chapman S. C., Smail I., Blain A. W., Ivison R. J., 2004, ApJ, 614, 671
Chapman S. C., Blain A. W., Smail I., Ivison R. J., 2005, ApJ, 622, 772
Chapman S. C., Blain A. W., Ibata R., Ivison R. J., Smail I., Morrison G., 2009, ApJ, 691, 560
Cimatti A. et al., 2004, Nat, 430, 184
Comastri A., 2004, in Barger A. J., ed., Astrophysics and Space Science Library Vol. 308, Supermassive Black Holes in the Distant Universe. Kluwer, Dordrecht, p. 245
Condon J. J., 1997, PASP, 109, 166
Condon J. J., Cotton W. D., Greisen E. W., Yin Q. F., Perley R. A., Taylor G. B., Broderick J. J., 1998, AJ, 115, 1693
Conselice C. J., Blackburne J. A., Papovich C., 2005, ApJ, 620, 564
Conselice C. J. et al., 2007, MNRAS, 381, 962
Conselice C. J., Rajgor S., Myers R., 2008, MNRAS, 386, 909
Cowie L. L., Barger A. J., Hu E. M., Capak P., Songaila A., 2004, AJ, 127, 3137
Daddi E., Cimatti A., Renzini A., Fontana A., Mignoli M., Pozzetti L., Tozzi P., Zamorani G., 2004, ApJ, 617, 746
Daddi E. et al., 2005, ApJ, 626, 680
Daddi E. et al., 2007, ApJ, 670, 173
Di Matteo T., Springel V., Hernquist L., 2005, Nat, 433, 604
Ellis S. C., O'Sullivan E., 2006, MNRAS, 367, 627
Elmegreen B. G., 1999, ApJ, 517, 103
Fabian A. C., Chapman S., Casey C. M., Bauer F., Blundell K. M., 2009, MNRAS, preprint (arXiv:0902.3117)

Fan X. et al., 2001, AJ, 121, 54
Fanaroff B. L., Riley J. M., 1974, MNRAS, 167, 31P
Frayer D. T. et al., 2006, ApJ, 647, L9
Gebhardt K. et al., 2000, ApJ, 539, L13
Holland W. S. et al., 1999, MNRAS, 303, 659
Hopkins P. F., Richards G. T., Hernquist L., 2007, ApJ, 654, 731
Kennicutt R. C. Jr, 1998, ApJ, 498, 541
Kormendy J., Richstone D., 1995, ARA&A, 33, 581
Lauer T. R., Tremaine S., Richstone D., Faber S. M., 2007, ApJ, 670, 249
Ledlow M. J., Owen F. N., 1996, AJ, 112, 9
Lehmer B. D. et al., 2007, ApJ, 657, 681
Lehmer B. D. et al., 2008, ApJ, 681, 1163
Magorrian J. et al., 1998, AJ, 115, 2285
Maraston C., 2005, MNRAS, 362, 799
McLure R. J., Jarvis M. J., Targett T. A., Dunlop J. S., Best P. N., 2006, MNRAS, 368, 1395
Merloni A., Heinz S., di Matteo T., 2003, MNRAS, 345, 1057
Muxlow T. W. B. et al., 2005, MNRAS, 358, 1159
Oke J. B. et al., 1995, PASP, 107, 375
Peng C. Y., Ho L. C., Impey C. D., Rix H.-W., 2002, AJ, 124, 266
Peng C. Y., Impey C. D., Rix H.-W., Kochanek C. S., Keeton C. R., Falco E. E., Lehár J., McLeod B. A., 2006, ApJ, 649, 616
Richards E. A., 2000, ApJ, 533, 611
Richards E. A., Fomalont E. B., Kellermann K. I., Windhorst R. A., Partridge R. B., Cowie L. L., Barger A. J., 1999, ApJ, 526, L73
Richards G. T. et al., 2006, AJ, 131, 2766
Steidel C. C., Shapley A. E., Pettini M., Adelberger K. L., Erb D. K., Reddy N. A., Hunt M. P., 2004, ApJ, 604, 534
Tacconi L. J. et al., 2006, ApJ, 640, 228
Thomasson P., 1986, QJRAS, 27, 413
Trujillo I., Conselice C. J., Bundy K., Cooper M. C., Eisenhardt P., Ellis R. S., 2007, MNRAS, 382, 109
van Dokkum P. G. et al., 2008, ApJ, 677, L5

This paper has been typeset from a TEX/LATEX file prepared by the author.